LAWRENCE
LIVERMORE
NATIONAL
LABORATORY

LLNL-JRNL-493114

Revealing deformation spectra of nanocrystalline nickel at elevated temperatures

Y. M. Wang, R. T. Ott, M. F. Besser, A. V. Hamza

August 12, 2011

Physical Review B

Disclaimer

Revealing deformation spectra of nanocrystalline nickel at elevated temperatures

Y.M. Wang[1], R.T. Ott[2], M.F. Besser[2], A.V. Hamza[1]

[1]Physical and Life Sciences Directorate, Lawrence Livermore National Laboratory, Livermore, CA 94550, USA

[2]Division of Materials Science and Engineering, Ames Laboratory (USDOE), Ames, Iowa 50011, USA

Abstract

In-situ synchrotron x-ray diffraction experiments have been performed to investigate the tensile deformation behavior of nanocrystalline nickel (~20 nm grain sizes) at elevated temperatures (150-300 ^{o}C) and high strain rates. The observed lattice strain deviations, average grain sizes, and dislocation densities at various stages of deformation and different temperatures suggest a strong dependence of dislocation slips and grain boundary sliding upon strain and temperature. Grain boundary migration has not yet dominated up to 300 ^{o}C.

Keywords: nanocrystalline nickel; in-situ synchrotron x-ray diffraction; tensile property; elevated temperatures; deformation mechanism.

Email: ymwang@llnl.gov

The deformation mechanism/behavior of nanocrystalline (nc) metals at elevated temperatures is an intriguing problem that bears great implications for superplastic formability of these high-strength materials, among which nc nickel is of particular interest as a model material for studying fundamental deformation physics. Recent mechanical testing results at elevated temperatures were generally rationalized by ex-situ transmission electron microscopy (TEM) observations[1-4], which is far from satisfactory due to microstructure evolution caused by residual heat and postmortem structural relaxation after unloading/fracture. As such, ex-situ techniques have difficulties in elucidating the competing deformation mechanisms (e.g., dislocation slips vs. twinning vs. grain boundary (GB) sliding) in nc materials. The in-situ TEM measurements[5-7] could overcome these issues; but the samples are considered too thin to be representative of the bulk behavior. The development of in-situ synchrotron x-ray diffraction (SXRD) techniques has greatly facilitated and broadened our understanding of the deformation behavior of bulk nc materials. However, previous experiments[8-11] were limited to room temperature and very slow strain rates ($<10^{-5}$ s^{-1}) primarily due to the slow data acquisition speed of x-ray detectors and the difficulty of controlling sample temperatures during in-situ SXRD experiments. To understand the superplastic deformability of nc materials and its relevant mechanisms, elevated temperatures and/or high strain rates are two key experimental parameters to explore as nc materials exhibit strong temperature and strain rate dependent deformation mechanisms[12].

In this letter, we report the in-situ SXRD results for tensile deformation of nc nickel (nominal average grain size, D~20 nm) at elevated temperatures of 150 – 300 ^{o}C and a relatively high strain rate of 1.4×10^{-3} s^{-1}. The microstructure details of this as-deposited nc nickel are described elsewhere with D~28±5 nm from plan-view TEM[13]. The nonmetallic impurities in the as-deposit are relevant for high-temperature deformation, which are measured to contain H (34),

C (91), P (30), S (310), and Si (<10) (all in ppm). Static thermal annealing or cycling experiments[4,14] have suggested that grain growth in nc nickel is negligible when the temperature is no more than 150 ^{o}C, whereas it becomes pronounced at the temperature above. Our in-situ SXRD experiments (performed at Sector 1-ID of the advanced Photon Source, Argonne National Laboratory) are thus designed to span these two temperature regions, where different deformation mechanisms can emerge. The bulk sample dimensions for all tensile tests are ~4.5 mm long × 2.0 mm wide × 0.12 mm thick. To achieve fast heating rates, we utilized an infrared heater, which can heat up the samples to the set point in a very short period of time (<120 s). Within the experimental conditions, surprisingly, fast grain growth and strong texture development in as-deformed samples are not observed, which only become pronounced after necking and an extended period of residual heating following fracture.

Fig. 1 shows the tensile engineering stress-strain curves of nc nickel, obtained at different temperatures from an in-situ synchrotron tensile frame (MTS 858). As expected, the 0.2% yield strength (σ_y) of nc nickel decreases with increasing temperatures, which are measured to be 897 MPa, 838 MPa, 467 MPa at room temperature (RT), 150 ^{o}C, 300 ^{o}C, respectively; i.e., a drastic drop of σ_y appears at 300 ^{o}C (see Table 1). The onset of a strong yield stress drop may suggest increasing GB activities; yet the conclusive experimental evidence has not been forthcoming. With decreasing strength, the tensile elongation to failure of nc nickel rises; but remains far below the superplastic values (i.e., >300%). Our independent strain rate jump tests indicate that the nc nickel has a strain rate sensitivity (m) value of 0.09 and 0.23 at 150 ^{o}C and 300 ^{o}C, respectively. This represents 4-10 folds increase compared to the typical m value (~0.02) measured at RT[12]. The marked increase of m may very well suggest a shift of deformation mechanisms at elevated temperatures. To decode the temperature-dependent plasticity in nc

nickel, we calculated the lattice strain deviations of (111), (200), (220), and (311) from the linear elasticity along the tensile axis, which is defined as $\Delta\varepsilon^{hkl} = \varepsilon^{hkl} - \varepsilon^{hkl}_{ref}$ (where ε^{hkl} is the measured lattice strain and ε^{hkl}_{ref} is the projected linear elastic lattice strain for a given reflection), and shown in Fig. 2 as a function of normalized stress (σ/σ_y) for three different temperatures. Note that the strain rate is fixed at ~1.4×10^{-3} s^{-1} and the x-ray exposures were collected in "real-time" during deformation. Interestingly, the characteristic shape of $\Delta\varepsilon^{hkl}$ for the sets of planes changes drastically from RT to 300 ^{o}C; i.e., from a conventional "Y" shape to an inverse "L" shape. This shape change indicates that the load partitioning among different crystallographic oriented grains and GBs transforms with the temperature. At 300 ^{o}C, it is found that the $\Delta\varepsilon^{hkl}$ of all planes initially exhibits a compressive shift (i.e., a negative $\Delta\varepsilon^{hkl}$) after yielding; but gradually turns back to the tensile direction. This is in contrast to the behavior at RT, whereas $\Delta\varepsilon^{hkl}$ of most planes remain compressive. Since the compressive shift in a crystallographic orientation represents plastic yielding and a decline in load sharing ability[15], the lattice strain deviation behavior at 300 ^{o}C suggests that grain interiors preferentially yield (rather than GBs) during the onset of plasticity[16]; but slowly become the chief load-carrier as $\Delta\varepsilon^{hkl}$ turns positive. Assuming GBs and grain interiors are the main load carriers, this finding infers that, at larger strains, GB activities switch the roles with grain interiors and start to make a dominant contribution to the plastic deformation of nc nickel.

At elevated temperatures, several different types of deformation mechanisms could occur in nc materials: (1) dislocation slips, which is a strongly thermally activated process in nc metals[12]; (2) GB sliding and diffusion, as predominately suggested by molecular dynamics simulations[17]; and (3) stress-driven (an athermal process)[18] or thermally activated, curvature-

driven GB migrations; or a combination of (2) and (3); e.g., the cooperative GB sliding and stress-driven GB migration process[19]; (4) Conventional or interface-controlled Coble creep is also considered important[1]. How these deformation processes compete with each other as the temperature arises is currently unknown. Process (3) is particularly intriguing, as it leads to grain growth and a loss of nc grain structure. The abundant literature[5,18] has suggested that rapid grain growth could become a dominant deformation mechanism in nc metals even at RT, which is expected to aggravate when the temperature arises. We have therefore calculated the average D as a function of the applied stress for samples deformed at 150 ^{o}C and 300 ^{o}C, respectively, using the modified Williamson-Hall method[9,20]. The grain growth was essentially not observed during the tests at both temperatures (see Table 1). The lack of grain growth at elevated temperatures may be related to the impurity pinning effects or the short period of heating and testing time (<3 mins.) in our experiments. No secondary phase such as Ni_3S_2 was detected by SXRD. The experimental results here suggest that GB migration mechanisms may have occurred at both temperatures; but have not yet dominated in our samples. The coherent shift of $\Delta\varepsilon^{hkl}$ towards tensile direction at larger strains is the direct evidence that GB sliding and diffusion play a more significant role in accommodating inhomogeneous plasticity of various grains in the late stage of deformation. This is supported by a large *m* value seen at 300 ^{o}C. However, the contribution of conventional Coble creep mechanism can be excluded from the measured activation volumes shown in Table 1.

To derive the contribution of dislocation slips to the overall plasticity of nc nickel, we use the SXRD peak broadening profiles and estimate dislocation density (ρ) during loading at different temperatures by fitting the equation[20]

$$(\Delta K)^2 = \left(\frac{0.9}{D}\right)^2 + \left(\frac{\pi b^2 \rho}{2A}\right) K^2 C \qquad (1),$$

where ΔK is the full width at half-maximum; b (=0.249 nm) is the Burgers vector of nickel; A is a constant that can be taken as 10; and C is a contrast factor that depends on the elastic anisotropy of the nickel. Table 1 summaries ρ results at different loading stages and temperatures. Despite obviously more ductile behavior at higher temperatures, ρ shows a decreasing trend with elevating temperatures due to strong dynamic recovery (so does the RMS strain after tests). These interesting results are in accord with our above view that GB sliding and diffusion contributes more significantly to the plastic deformation at higher strains and higher temperatures.

To gain a thorough picture of the deformation process at elevated temperatures, we have documented the texture evolution (from peak intensity of SXRD), fracture pattern (scanning electron microscopy), nanovoids content (ultra-small-angle x-ray scattering, USAXS)[13], and postmortem grain structure (focused-ion-beam ion-channeling method) of nc nickel. Provided that the plasticity was mainly carried by dislocation slips, strong texture development is expected at larger strains. Of all the planes we examined (i.e., 111, 200, 220, 311) (two examples are shown in Figs. 3a-b), however, texture development is negligible during the loading at both temperatures, which is also consistent with the lack of grain growth. At 300 ^{o}C, a sudden increase of (111) peak intensity along the tensile axis is observed when necking starts to set in (Fig. 3b), likely due to the larger strains in this region caused by complicated triaxial stresses. This result suggests that the final necking process could substantially impact the microstructure of samples. Examinations of fracture patterns at three different temperatures indicate that dimple sizes increase drastically with elevating temperatures, Figs. 3c-d and Table 1. Some large voids

are also found in 300 ^{o}C-deformed samples, the postmortem grain structures of which generally exhibit a bimodal distribution, Fig. 3e; but grains are nonuniform in different regions and not elongated, either. Significantly, we find that ex-situ grain growth is more severe near the necking area. These results indicate the microstructure complexity of high-temperature-deformed nc materials. Some discrepancies seen from ex-situ characterizations[1,3,4] and in-situ SXRD interpretations may be attributed to the following important factors: (1) residual heat and necking caused further grain growth, which was not accounted for in most previous experiments; (2) the grain size derived from the modified Williamson-Hall equation may represent the lower bound of D, as large grains contribute negligibly to the peak broadening; (3) as indicated in Fig. 3e, the grain structure in as-deformed samples is distributed non-uniformly, which affects ex-situ TEM sampling, as well as in-situ SXRD measurements (i.e., depending on the location of beams). Nevertheless, our results here suggest a number of unique advantages of using in-situ SXRD technique to elucidate the dynamic and competing deformation processes in nc materials.

In summary, we have investigated the deformation physics of nc nickel at elevated temperatures and high strain rates. The in-situ SXRD results help to reveal several competing deformation mechanisms in nc nickel, which is a strong function of strain and temperature. We find that, with elevating temperatures, dislocation density decreases upon loading, whereas GB sliding and diffusion play increasing roles in contributing the tensile plasticity of nc materials. Strong grain growth and texture development are not observed for both temperatures, consistent with GB sliding and diffusion mechanisms.

Acknowledgement

This work was performed under the auspices of the U.S. Department of Energy by Lawrence Livermore National Laboratory under Contract DE-AC52-07NA27344. The work at Ames Laboratory was supported by the U.S. Department of Energy, Office of Basic Energy Science, Division of Materials Sciences and Engineering under Contract No. DE-AC02-07CH11358. We thank Dr. J. Almer for his assistance with in-situ SXRD experiments and Dr. M. J. Kramer for the helpful discussions. The APS was supported by the U.S. Department of Energy under Contract DE-AC02-06CH11357.

References

[1] M. J. N. V. Prasad and A. H. Chokshi, Acta Mater. **58**, 5724 (2010).

[2] S. X. McFadden, R. S. Mishra, R. Z. Valiev, A. P. Zhilyaev, and A. K. Mukherjee, Nature **398**, 684 (1999).

[3] F. Dalla Torre, H. Van Swygenhoven, R. Schaublin, P. Spatig, and M. Victoria, Scr. Mater. **53**, 23 (2005).

[4] Y. M. Wang, S. Cheng, Q. M. Wei, E. Ma, T. G. Nieh, and A. Hamza, Scr. Mater. **51**, 1023 (2004).

[5] T. J. Rupert, D. S. Gianola, Y. Gan, and K. J. Hemker, Science **326**, 1686 (2009).

[6] L. H. Wang, X. D. Han, P. Liu, Y. H. Yue, Z. Zhang, and E. Ma, Phys. Rev. Lett. **105**, 135501 (2010).

[7] Z. W. Shan, J. M. K. Wiezorek, E. A. Stach, D. M. Follstaedt, J. A. Knapp, and S. X. Mao, Phys. Rev. Lett. **98**, 095502 (2007).

[8] Z. Budrovic, H. Van Swygenhoven, P. M. Derlet, S. Van Petegem, and B. Schmitt, Science **304**, 273 (2004).

[9] Y. M. Wang, R. T. Ott, A. V. Hamza, M. F. Besser, J. Almer, and M. J. Kramer, Phys. Rev. Lett. **105**, 215502 (2010).

[10] C. D. Grant, J. C. Crowhurst, T. Arsenlis, E. M. Bringa, Y. M. Wang, J. A. Hawreliak, P. J. Pauzauskie, and S. M. Clark, J. Appl. Phys. **105**, 6 (2009).

[11] H. Q. Li, H. Choo, Y. Ren, T. A. Saleh, U. Lienert, P. K. Liaw, and F. Ebrahimi, Phys. Rev. Lett. **101**, 015502 (2008).

[12] Y. M. Wang, A. V. Hamza, and E. Ma, Acta Mater. **54**, 2715 (2006).

[13] Y. M. Wang, R. T. Ott, T. van Buuren, T.M. Willey, M. M. Biener, and A.V. Hamza, Phys. Rev. B, submitted (2011).

[14] J. Lohmiller, C. Eberl, R. Schwaiger, O. Kraft, and T. J. Balk, Scr. Mater. **59**, 467 (2008).

[15] C. C. Aydiner, D. W. Brown, N. A. Mara, J. Almer, and A. Misra, Appl. Phys. Lett. **94**, 031906 (2009).

[16] Y. M. Wang, A. V. Hamza, and T. W. Barbee, Appl. Phys. Lett. **91**, 061924 (2007).

[17] Y. J. Wei, A. F. Bower, and H. J. Gao, Acta Mater. **56**, 1741 (2008).

[18] K. Zhang, J. R. Weertman, and J. A. Eastman, Appl. Phys. Lett. **87**, 061921 (2005).

[19] S. V. Bobylev, N. F. Morozov, and I. A. Ovid'ko, Phys. Rev. Lett. **105**, 055504 (2010).

[20] T. Ungar, I. Dragomir, A. Revesz, and A. Borbely, J. Appl. Crystallogr. **32**, 992 (1999).

Figure captions

Figure 1 (color online) Tensile engineering stress-strain curves of nc nickel at RT, 150 ^{o}C, and 300 ^{o}C, respectively.

Figure 2 (color online) The lattice strain deviations ($\Delta\varepsilon^{hkl}$) of nc nickel as a function of normalized stress (σ/σ_y) at RT, 150 ^{o}C, and 300 ^{o}C, respectively. Note the difference of overall $\Delta\varepsilon^{hkl}$ shape.

Figure 3 (color online) Texture, fracture surface, and grain structures in nc nickel. (a) and (b), (111) texture evolution as a function of applied stress for samples tested at 150 ^{o}C and 300 ^{o}C, respectively. The stress increment follows red to green to blue. The angle, ϕ, represents the angle between the diffracting plane and the tensile loading axis. The plots have been normalized to the peak intensity of the unloaded sample, and therefore, represent changes in intensity during deformation. Note the sudden increase of the intensity in the peaks oriented normal to the tensile axis at 300 ^{o}C after necking; (c) and (d), dimple features for samples tested at 150 ^{o}C and 300 ^{o}C, respectively; (e), bimodal grain structure observed in 300 ^{o}C-tested sample. The fracture surface is on the top side of this image, where nearby grains appear larger.

Table 1 A summary of the tensile properties of nc nickel from RT to 300 ^{o}C, at the strain rate of ~1.4×10^{-3} s^{-1}. The activation volume is calculated according to $V = \frac{\sqrt{3}kT}{m\sigma}$, where k is the Boltzmann constant, T is the temperature, and σ is the flow stress. The maximum (ρ_{max}) and residual dislocation densities (ρ_{rsd}) refer to the dislocation density at the peak load and after fracture, respectively.

	RT	150 ^{o}C	300 ^{o}C
$\sigma_{0.2}$ (MPa)	897	838	467
Strain rate sensitivity (m)	0.02	0.09	0.23
Activation volume (V)	$26b^3$	$9b^3$	$8b^3$
Grain size (nm) before loading (from SXRD)	~20	~20	~20
Grain size (nm) after fracture (from SXRD)	~21	~22	~25
Residual RMS strain (%) after test	0.48	0.28	0.17
ρ_{max} (m^{-2})	4.50×10^{15}	4.45×10^{15}	2.62×10^{15}
ρ_{rsd} (m^{-2})	2.89×10^{15}	2.49×10^{15}	1.02×10^{15}
Dimple size (μm)	0.5-1.5	0.8-2.0	1.2-3.5

Figure 1

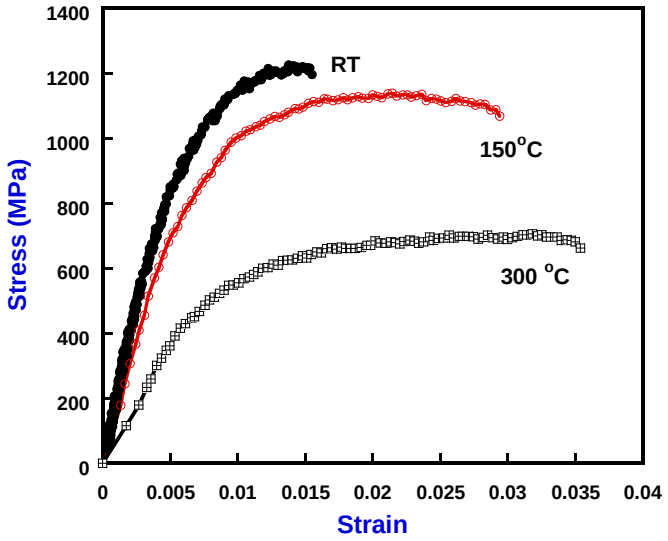
1400
1200
1000
800
600
400
200
0
Stress (MPa)
0
0.005
0.01
0.015
0.02
0.025
0.03
0.035
0.04
Strain
RT
150°C
300 °C

Figure 2

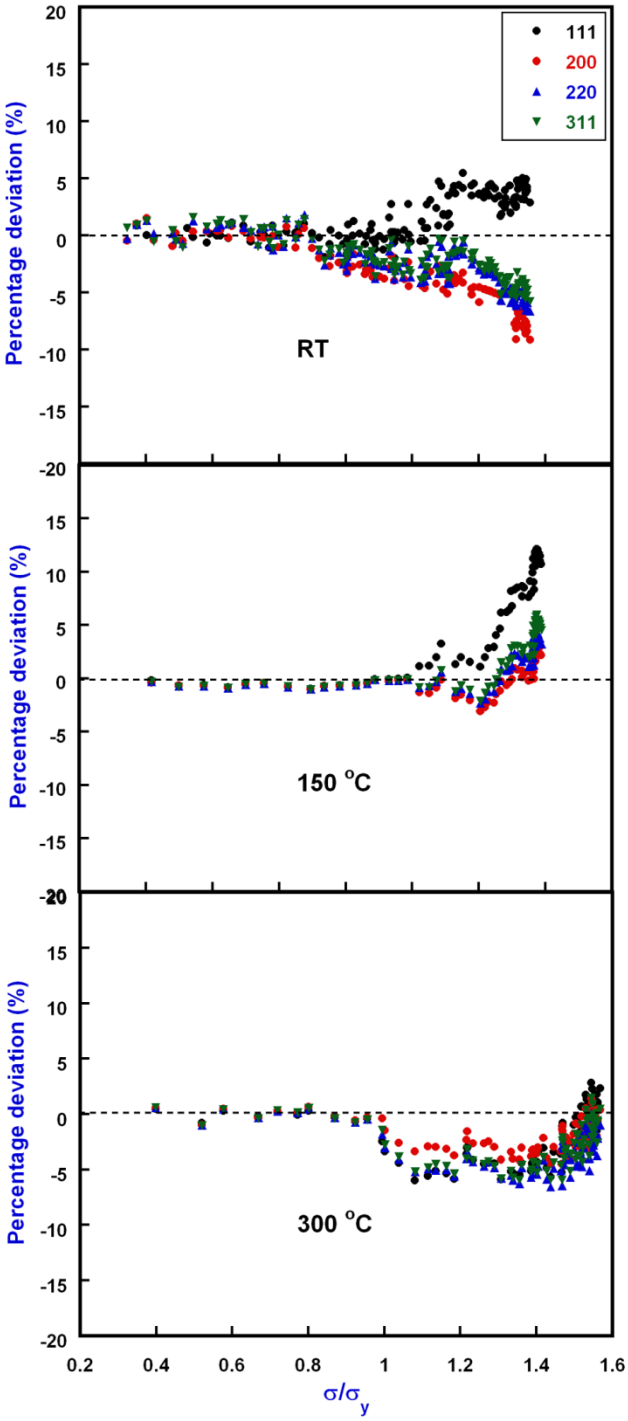

Figure 3